Frascati Physics Series Vol. LVI (2012)
Dark Forces at Accelerators
October 16-19, 2012

SEARCH FOR DARK HIGGSSTRAHLUNG PROCESSES AT KLOE

Enrico Graziani
INFN sezione di Roma Tre, Roma, Italy
on behalf of the KLOE/KLOE2 Collaboration *

* D. Babusci, D. Badoni, I. Balwierz-Pytko, G. Bencivenni, C. Bini, C. Bloise, F. Bossi, P. Branchini, A. Budano, L. Caldeira Balkeståhl, G. Capon, F. Ceradini, P. Ciambrone, F. Curciarello, E. Czerwiński, E. Dané, V. De Leo, E. De Lucia, G. De Robertis, A. De Santis, P. De Simone, A. Di Domenico, C. Di Donato, R. Di Salvo, D. Domenici, O. Erriquez, G. Fanizzi, A. Fantini, G. Felici, S. Fiore, P. Franzini, P. Gauzzi, G. Giardina, S. Giovannella, F. Gonnella, E. Graziani, F. Happacher, L. Heijkenskjöld, B. Höistad, L. Iafolla, E. Iarocci, M. Jacewicz, T. Johansson, K. Kacprzak, W. Kluge, A. Kupsc, J. Lee-Franzini, F. Loddo, P. Lukin, G. Mandaglio, M. Martemianov, M. Martini, M. Mascolo, R. Messi, S. Miscetti, G. Morello, D. Moricciani, P. Moskal, S. Muller, F. Nguyen, A. Passeri, V. Patera, I. Prado Longhi, A. Ranieri, C. F. Redmer, P. Santangelo, I. Sarra, M. Schioppa, B. Sciascia, M. Silarski, C. Taccini, L. Tortora, G. Venanzoni, R. Versaci, W. Wiślicki, M. Wolke, J. Zdebik

Abstract

We searched for the existence of a Higgstrahlung process in a secluded sector, possibly leading to a dark photon and a dark Higgs final state. Using the KLOE detector at the DAΦNE e^+e^- collider in Frascati, we investigated the case in which the dark Higgs boson h' is lighter than the dark photon U and thus escapes detection, showing up as a missing energy, and the dark photon U decays in a muon pair. We found no evidence of the process and set tight upper limits to its parameters.

1 Introduction

In recent years, several unexpected astrophysical observations have failed to find a common interpretation in terms of standard astrophysical or particle physics sources. A non exhaustive list of these observations include the 511 keV gamma-ray signal from the galactic center observed by the INTEGRAL satellite [1)], the excess in cosmic ray postirons reported by PAMELA [2)], the total electron and positron flux measured by ATIC [3)], Fermi [4)], and HESS [5, 6)], the annual modulation of the DAMA/LIBRA signal [7, 8)] and the low energy spectrum of nuclear recoil candidate events observed by CoGeNT [9)].

Although there are alternative explanations for some of these anomalies, they could be all explained with the existence of a dark matter weakly interacting massive particle, WIMP, belonging to a secluded gauge sector under which the Standard Model (SM) particles are uncharged [10−19)] An abelian gauge field, the U boson with mass near the GeV scale, couples the secluded sector to the SM through its kinetic mixing with the SM hyper-charge gauge field. The kinetic mixing parameter ϵ is expected to be of the order $10^{-4} - 10^{-2}$ [11−20)] so that observable effects can be induced in O(GeV)-energy e^+e^- colliders [20−24)] and fixed target experiments [25−28)] .

The U boson can be produced at e^+e^- colliders via different processes: $e^+e^- \to U\gamma$, $e^+e^- \to Uh'$ (dark Higgsstrahlung), where h' is a Higgs-like particle responsible for the breaking of the hidden symmetry, and $V \to P\gamma$ decays, where V and P are vector and pseudoscalar mesons, respectively. In this work we study the Higgsstrahlung process $e^+e^- \to Uh'$ using data collected by the KLOE experiment at the e^+e^- collider DAΦNE at Frascati, both at a center of mass energy of $\sim$ 1019 MeV, the mass of the Φ meson (on peak sample), and at a center of mass energy of $\sim$ 1000 MeV (off peak sample).

The process $e^+e^- \to Uh'$ is one of the most interesting reactions to study at an e^+e^- collider because, differently from the other final states listed above, is suppressed by a single factor of ϵ. There are two very different scenarios depending on the masses of the dark photon and of the dark Higgs boson. For Higgs boson mass $m_{h'}$ larger than two dark photon masses m_U, the dark Higgs boson would decay dominantly and promptly to a U boson pair, thus giving rise to a six charged particle final state (this case was recently investigated by the BaBar experiment [29]); while Higgs bosons lighter than the dark photon would have, in most of the parameter space region, such a large lifetime to escape undetected, showing up as a missing energy signature. In this work we study only the so called "invisible" dark Higgs scenario, thus confining our search to the case $m_{h'} < m_U$.

The lifetime of the dark Higgs boson depends on the kinetic mixing parameter ϵ, the boson masses $m_{h'}$ and m_U and the dark coupling constant α_D. For masses of the order of 100 MeV and $\alpha_D = \alpha_{em}$ the dark Higgs boson lifetime would be $\sim 5\mu s$ for $\epsilon \sim 10^{-3}$, corresponding, for KLOE energies, to a decay length of $\sim$ 100 m. The dark Higgs boson would be invisible up to $\epsilon \sim 10^{-2} \div 10^{-1}$, depending on the h' mass.

We limit our search to the decay of the U boson in a muon pair: our final state signature is then a couple of opposite charge muons plus missing energy. The measurement is thus performed in the range $2m_\mu < m_U < 1000$ MeV with the constraint $m_{h'} < m_U$.

The production cross section of the dark Higgsstrahlung process is proportional to the product $\alpha_D \times \epsilon^2$ and depends on the boson masses [21]. Fig.1 shows the expected cross section in the KLOE range of interest, for $\epsilon = 10^{-3}$ and $\alpha_D = \alpha_{em}$, as a function of $m_{h'}$ and m_U. Values as high as hundreds of fb are reachable in this hypothesis. Compared to the B-factory case [29], KLOE benefits of the 1/s factor and of the resonance-like behaviour expected for the producion cross section [21].

2 The KLOE detector

The KLOE experiment operated from 2000 to 2006 at DAΦNE, the Frascati Φ factory. DAΦNE is an e^+e^- collider running mainly at a center-of-mass energy of $\sim$1019 MeV, the mass of the Φ meson. Equal energy positron and electron beams collide at an angle of $\sim$ 25 mrad, producing Φ mesons nearly at rest. The

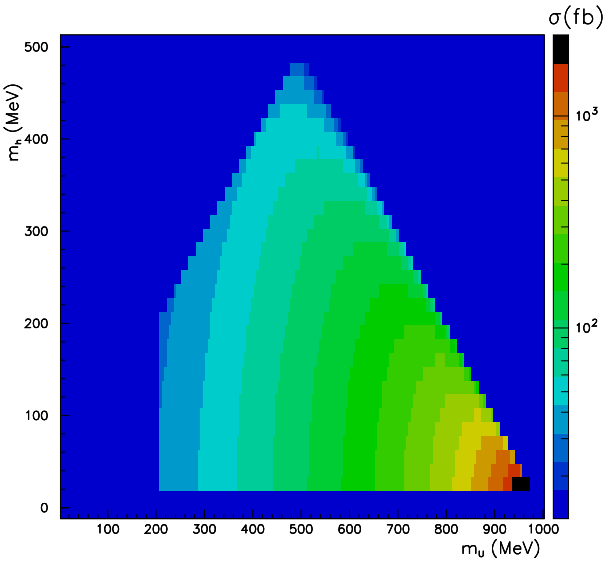

Figure 1: *Dark Higgsstrahlung production cross section for* $\epsilon = 10^{-3}$ *and* $\alpha_D = \alpha_{em}$ *as a function of* $m_{h'}$ *and* m_U.

detector consists of a large cylindrical Drift Chamber (DC), surrounded by a lead-scintillating fiber electromagnetic calorimeter (EMC). A superconducting coil around the EMC provides a 0.52 T field. The beam pipe at the interaction region is spherical in shape with 10 cm radius, it is made of a beryllium-aluminum alloy of 0.5 mm thickness. Low beta quadrupoles are located at about ±50 cm distance from the interaction region. The drift chamber [30], 4 m in diameter and 3.3 m long, has 12,582 all-stereo tungsten sense wires and 37,746 aluminum field wires. The chamber shell is made of carbon fiber-epoxy composite with an internal wall of $\sim$ 1 mm thickness, the gas used is a 90% helium, 10% isobutane mixture. The spatial resolutions are $\sigma_{xy} \sim 150\mu m$ and $\sigma_z \sim 2$ mm. The momentum resolution is $\sigma_\perp/p_\perp \approx 0.4$ %. Vertexes are reconstructed with a spatial resolution of ~ 3 mm. The calorimeter [31] is divided into a barrel and two endcaps, for a total of 88 modules, and covers 98% of the solid angle. The modules are read out at both ends by photomultipliers,

both in amplitude and time. The readout granularity is $\sim$ (4.4.4) cm^2, for a total of 2440 cells arranged in five layers. The energy deposits are obtained from the signal amplitude while the arrival times and the particles positions are obtained from the time differences. Cells close in time and space are grouped into energy clusters. The cluster energy E is the sum of the cell energies. The cluster time T and position are energy-weighted averages. Energy and time resolutions are $\sigma_E/E = 5.7\%/\sqrt{E(GeV)}$ and $\sigma_t = 57$ ps$/\sqrt{E(GeV)} \oplus 100$ ps, respectively. The trigger [32] uses both calorimeter and chamber information. In this analysis the events are selected by the calorimeter trigger, requiring two energy deposits with E>50 MeV for the barrel and E>150 MeV for the endcaps. A cosmic veto rejects events with at least two energy deposits above 30 MeV in the outermost calorimeter layer. Data are then analyzed by an event classification filter [33] , which selects and streams various categories of events in different output files.

3 Event selection

The analysis of the process $e^+e^- \to Uh'$, $U \to \mu^+\mu^-$, h' invisible, has been performed on a data sample of 1.65 fb^{-1} collected during the 2004-2005 KLOE data taking campaign at a center of mass energy of $\sim$ 1019 MeV, corresponding to the mass of the Φ meson (on peak sample), and on a data sample of 0.2 fb^{-1} at a center of mass energy of $\sim$ 1000 MeV (off peak sample), well below the Φ resonance.

The Monte Carlo simulation of the signal process $e^+e^- \to Uh'$, $U \to \mu^+\mu^-$, h' invisible, has been produced using an ad hoc generator interfaced with the standard Geanfi KLOE full simulation program. A grid in $m_{h'}$ - m_U masses, with approximate steps of $\sim$ 30 MeV has been generated to cover all the allowed region. The mass resolution was found to be between 0.5 and 2 MeV for m_U (invariant mass of the muon pair) and between 3 and 17 MeV for $m_{h'}$ (missing mass). The signature of the process would thus be the appearance of a sharp peak in the bidimensional distribution $M_{\mu\mu}$ - M_{miss}. We define θ as the polar angle direction of the muon pair momentum (momentum of the U boson, opposite to that of the h', in case of dark Higgsstrahlung events). Contrarily to most of the dominant QED background processes, the signal is predicted to show a large angle production in θ, with two dominant terms proportional to $sin\theta$ and $sin^3\theta$ [21].

As a first step of the analysis, a preselection was performed by requiring:

- events with only two opposite charge tracks, with a reconstructed vertex inside a 4×30 cm cylinder around the interaction point;
- each track must have an associated EMC cluster;
- the visible momentum direction has to be in the barrel: $|cos\theta| < 0.75$;
- the momenta of the two tracks must be individually below 460 MeV;
- the modulus of the missing momentum must exceed 40 MeV.

After this selections (mostly aimed at rejecting QED backgrounds), the hermeticity and tightness of the electromagnetic calorimeter was used as a veto to avoid the presence of photons in the event. It was required to have no unassociated energy deposition with E>15 MeV on EMC. The inefficiency of the calorimeter as a function of the energy was studied with a sample of radiative Bhabhas $e^+e^- \to e^+e^-\gamma$ reconstructed with the DC only, with the missing momentum direction (corresponding to the direction of the photon) pointing to the barrel: $|cos\theta| < 0.75$. It was found that the EMC inefficiency in photon detection started below 10% level at 20 MeV, to fall down to $\sim 1\%$ at ~ 70 MeV and to 0.1% at ~ 200 MeV.

The event selection then proceeded by applying particle identification (PID) algorithms to the two charged tracks. These were almost entirely based on the excellent energy and time resolution of the EMC. A set of neural network, organised for different values of track momentum and polar angle, was trained on simulated Monte Carlo samples to perform muon to electron discrimination. The neural networks used five input variables (three of them related with energy depositions in calorimeter planes, i.e. the longitudinal shower profile, energy to momentum ratio, cluster time, related to the time of flight and thus to the particle velocity) and one output. The PID performances, checked on selected data samples of $e^+e^- \to e^+e^-$, $e^+e^- \to \mu^+\mu^-$, $e^+e^- \to \pi^+\pi^-$ were found to be excellent: the fraction of $e^+e^- \to \mu^+\mu^-$ events, in which both tracks were required to be identified as muons, was measured to be 85%, while the fraction of residual $e^+e^- \to e^+e^-$ events was 10^{-4} and the fraction of doubly tagged $e^+e^- \to \pi^+\pi^-$ was $\sim 50\%$ (muon and pion induced showers look very similar at KLOE energies).

After the missing energy and the PID selections, a huge background from $\Phi \to K^+K^-$, $K^\pm \to \mu^\pm\nu$ events survives in the on peak sample. This corresponds to the fraction of doubly early leptonically decaying charged kaons in the IP region. Charged kaons have in KLOE an average decay length of ~ 90 cm. The reconstructed vertex of the extrapolated muon tracks is thus expected to be displaced from the IP, due to the charged kaon lifetime, and with a bad χ^2 of the fitting procedure. Cuts on the radial and z projections of the distance between the reconstructed vertex and the IP and on the χ^2 of the fit allowed to reduce by a factor ~ 35 the $\Phi \to K^+K^-$, $K^\pm \to \mu^\pm\nu$ background.

Events surviving all the described selections were organized in bidimensional histograms with the muon pair mass $M_{\mu\mu}$ and the event missing mass M_{miss} on the two axes. The binning was chosen such as to keep most of the signal in one bin only. In $M_{\mu\mu}$ a 5 MeV bin width was enough over all the plane; while for M_{miss} a variable binning of 15, 30 and 50 MeV widths was chosen. According to the simulation, a fraction of $90\div95\%$ of the signal was contained in one bin. The selection efficiency, estimated from the Monte Carlo on the generated points of the m_U-$m_{h'}$ grid, was found to be between 15% and 25%, depending on the masses, with most frequent values $\sim$20%. The efficiency for a generic point on the $M_{\mu\mu}$-M_{miss} plane was then evaluated by linear interpolation between the two closest available generated points lying on opposite sides of the considered one.

Several sources of systematic uncertainties in the signal efficiency evaluation were taken into account. Uncertainties from the PID procedure were estimated by selecting samples of $e^+e^- \to \mu^+\mu^-\gamma$ in data and Monte Carlo, applying the PID algorithms to them and studing the differences between the samples. The results were used first to correct the Monte Carlo efficiency as a function of the track momentum and then to quote a systematic uncertainty, assumed to be of the order of the average correction. An 8% effect was ascribed to this source. The same $e^+e^- \to \mu^+\mu^-\gamma$ samples selected in data and in the simulation were used to evaluate the effect of the cut on the vertex-IP distance. A 12% average difference was found and used to correct the Monte Carlo efficiency. A 3% effect due to the spread of this correction as a function of the missing momentum polar angle direction was assigned to this source. The systematic uncertainty due to the usage of the EMC veto was evaluated by selecting samples of $\Phi \to K^+K^-$, $K^\pm \to \mu^\pm\nu$ in data and Monte Carlo. In this case, the cut on the vertex-IP distance was removed to increase the size of

the statistical sample. A 2% difference was observed and used both to correct the Monte Carlo efficiency and to quote a systematic uncertainty due to this source. Finally, a 5% uncertainty was estimated due to interpolation and binning effects in the efficiency evaluation procedure. A total $\pm 10\%$ systematic uncertainty was then evaluated as the quadratic sum of all the above effects.

4 Results

Results are shown in fig.2 for the on peak and off peak samples respectively. In the left plot of fig.2 (on peak sample) several sources of backgrounds are easily distinguishable: $\Phi \to K^+K^-$, $K^\pm \to \mu^\pm\nu$ (triangular region at the left of the populated part of the distribution), $\Phi \to \pi^+\pi^-\pi^0$ (mostly horizontal band, corresponding to events in which both photons from π^0 decay are undetected), continuum backgrounds $e^+e^- \to \mu^+\mu^-$ and $e^+e^- \to \pi^+\pi^-$ (diagonal bands starting from the right-bottom part of the distribution), $e^+e^- \to e^+e^-\mu^+\mu^-$ and $e^+e^- \to e^+e^-\pi^+\pi^-$ (two photon events, top part of the distribution, for $M_{miss} > 350MeV$). In the distribution in the right plot of fig.2 (off peak sample) all the backgrounds from the Φ decays are strongly suppressed.

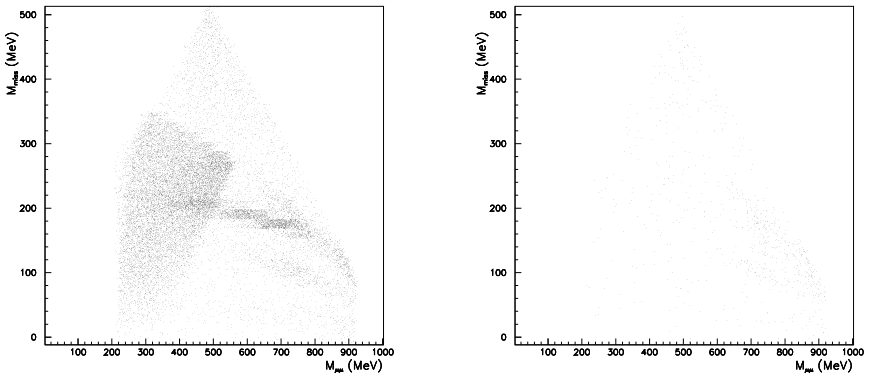

Figure 2: *Results for on peak sample (left plot, 1.65 fb^{-1} integrated luminosity) and off peak sample (right plot, 0.2 fb^{-1} integrated luminosity).*

In order to search for possible signals or to set upper limits to the production of the dark Higgsstrahlung process, an accurate estimate of the background

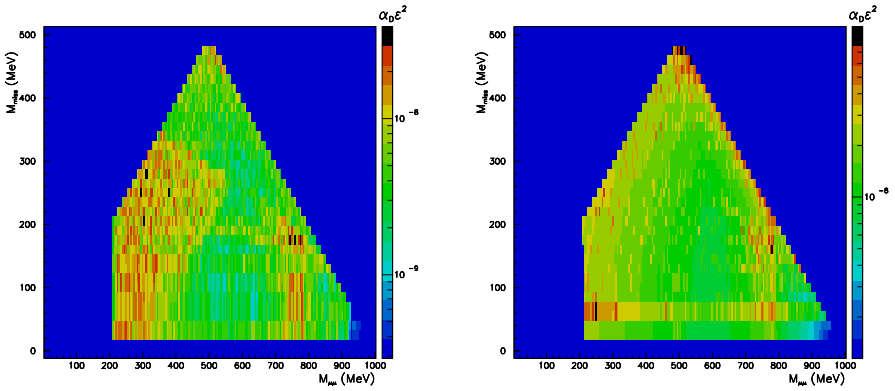

Figure 3: *90% CL upper limits in $\alpha_D \times \epsilon^2$ for the on peak sample (left plot) and off peak sample (right plot).*

is needed. At the time of the workshop, mostly for technical problems, a complete Monte Carlo simulation for all the contributing background processes was not available. The background was then evaluated directly on the data. A 5×5 bin matrix in the $M_{\mu\mu}$-M_{miss} plane was built and moved all along the populated regions of fig.2. The average of the content of the 24 bins surrounding the central one, where the presence of a possible signal is checked, was assumed to be an estimate of its background. No evidence of the dark Higgsstrahlung process was found. Using uniform prior distributions, 90% confidence level Bayesian upper limits on the number of events were derived bin by bin, separately for the on peak and off peak samples. These results were then converted in terms of the dark Higgstrahlung production cross section parameters $\alpha_D \times \epsilon^2$ by using:

- the integrated luminosity information;
- the signal efficiency as described above;
- the dark Higgsstralung cross section and the branching fraction of the U boson decay into muon pairs as in reference [21];

The small fraction of the signal outside the central bin of the 5×5 matrix was explicitly taken into account into the likelihood expression. The 10% systematic

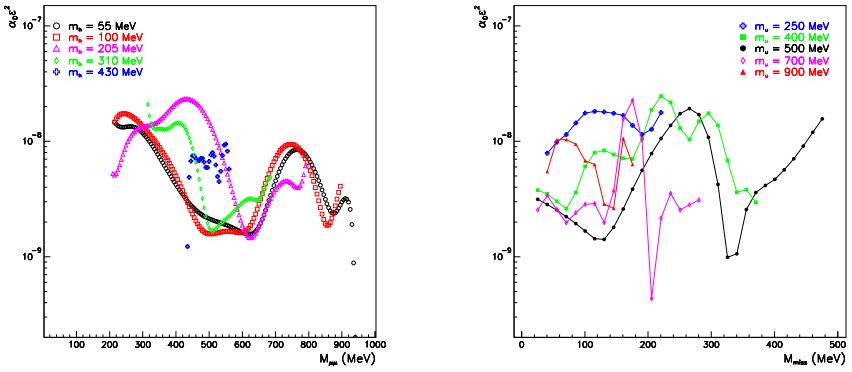

Figure 4: *Combined 90% CL upper limits in $\alpha_D\epsilon^2$ as a function of $M_{\mu\mu}$ for different values of $m_{h'}$ (left plot) and as a function of M_{miss} for different values of m_U (right plot).*

uncertainties on the signal efficiency were taken into account by convolving the likelihood with gaussian distributions with variances set equal to the estimated systematic errors. The $\alpha_D \times \epsilon^2$ 90% CL limits are shown in fig.3 separately for the on peak and off peak sample. These results were then combined by taking into account the different integrated luminosities of the two samples and the expected slightly different signal efficiencies and cross sections due to the different center of mass energies. The combined 90% CL upper limits were then projected in the $M_{\mu\mu}$ and M_{miss} directions and slightly smoothed, just to make them more readable. They are shown in fig.4. These limits are largely dominated by the available data statistics. Values as low as $10^{-9} \div 10^{-8}$ in $\alpha_D\epsilon^2$ are excluded at 90% CL for a large range of the dark photon and dark Higgs masses.

5 Conclusions

A search for the dark Higgsstrahlung process has been performed by KLOE in the range $2m_\mu < m_U < 1000$ MeV with $m_{h'} < m_U$. No signal has been observed and upper limits on the product of the mixing angle and the dark coupling constant have been set in the range $10^{-9} \div 10^{-8}$ in $\alpha_D\epsilon^2$. Assuming

$\alpha_D = \alpha_{em}$ these measurements translate into limits on the mixing angle in the range $10^{-4} \div 10^{-3}$. These results are numerically comparable with those of Babar [29] and complement them as they refer to the same process in a different final state and in a different region of the phase space.

At KLOE2/DAΦNE2 the larger expected integrated luminosity and the presence of a high resolution Inner Tracker detector are expected to improve these results at least by a factor 2, thus allowing a study deep inside the $\epsilon \approx 10^{-4}$ parameter space region.

References

1. P.Jean *et al*, Astron. Astrophys., **407** (2003), p. L55
2. O. Adriani *et al.* Nature, **458** (2009), p. 607
3. J. Chang *et al.* Nature, **456** (2008), p. 362
4. A.A. Abdo *et al.* Phys. Rev. Lett., **102** (2009), p. 181101
5. F. Aharonian *et al.* Phys. Rev. Lett., **101** (2008), p. 261104
6. F. Aharonian *et al.* Astron. Astrophys., **508** (2009), p. 561
7. R. Bernabei *et al.* Int. J. Mod. Phys. D, **13** (2004), p. 2127
8. R. Bernabei *et al.* Eur. Phys. J. C, **56** (2008), p. 333
9. C.E. Aalseth *et al.* Phys. Rev. Lett., **107** (2011), p. 141301
10. M. Pospelov, A. Ritz, M.B. Voloshin Phys. Lett. B, **662** (2008), p. 53
11. N. Arkani-Hamed, D.P. Finkbeiner, T.R. Slatyer, N. Weiner Phys. Rev. D, **79** (2009), p. 015014
12. D.S.M. Alves, S.R. Behbahani, P. Schuster, J.G. Wacker Phys. Lett. B, **692** (2010), p. 323
13. M. Pospelov, A. Ritz Phys. Lett. B, **671** (2009), p. 391
14. J. Hisano, S. Matsumoto, M.M. Nojiri Phys. Rev. Lett., **92** (2004), p. 031303

15. M. Cirelli, M. Kadastik, M. Raidal, A. Strumia Nucl. Phys. B, **813** (2009), p. 1

16. J. March-Russell, S.M. West, D. Cumberbatch, D. Hooper JHEP, **0807** (2008), p. 058

17. I. Cholis, G. Dobler, D.P. Finkbeiner, L. Goodenough, N. Weiner Phys. Rev. D, **80** (2009), p. 123518

18. I. Cholis, D.P. Finkbeiner, L. Goodenough, N. Weiner JCAP, **0912** (2009), p. 007

19. N. Arkani-Hamed, N. Weiner JHEP, **0812** (2008), p. 104

20. R. Essig, P. Schuster, N. Toro Phys. Rev. D, **80** (2009), p. 015003

21. B. Batell, M. Pospelov, A. Ritz Phys. Rev. D, **79** (2009), p. 115008

22. M. Reece, L.T. Wang JHEP, **0907** (2009), p. 051

23. N. Borodatchenkova, D. Choudhury, M. Drees Phys. Rev. Lett., **96** (2006), p. 141802

24. P.F. Yin, J. Liu, S.h. Zhu Phys. Lett. B, **679** (2009), p. 362

25. J.D. Bjorken, R. Essig, P. Schuster, N. Toro Phys. Rev. D, **80** (2009), p. 075018

26. B. Batell, M. Pospelov, A. Ritz Phys. Rev. D, **80** (2009), p. 095024

27. R. Essig, P. Schuster, N. Toro, B. Wojtsekhowski JHEP, **1102** (2011), p. 009

28. M. Freytsis, G. Ovanesyan, J. Thaler JHEP, **1001** (2010), p. 111

29. J.P. Lees *et al.* (BaBar Collab.) Phys. Rev. Lett. **108** (2012) 211801

30. M. Adinolfi *et al.* Nucl. Instr. Meth. A, **488** (2002), p. 51

31. M. Adinolfi *et al.* Nucl. Instr. Meth. A, **482** (2002), p. 364

32. M. Adinolfi *et al.* Nucl. Instr. Meth. A, **492** (2002), p. 134

33. F. Ambrosino *et al.* Nucl. Instr. Meth. A, **534** (2004), p. 403